The Astrophysical Journal, 640:L99–L102, 2006 March 20

JETS OF ENERGETIC PARTICLES GENERATED BY MAGNETIC RECONNECTION AT A THREE-DIMENSIONAL MAGNETIC NULL

S. Dalla and P. K. Browning
School of Physics and Astronomy, University of Manchester, P.O. Box 88, Manchester M60 1QD, UK
Received 2006 January 10; accepted 2006 February 10; published 2006 March 6

ABSTRACT

We investigate particle acceleration during magnetic reconnection at a three-dimensional magnetic null point, in the spine reconnection regime, using a test particle numerical code. We observe efficient particle acceleration and find that two energetic populations are produced: a trapped population of particles that remain in the vicinity of the null and an escaping population, which leave the configuration in two symmetric jets along field lines near the spine. While the parameters used in our simulation aim to represent solar coronal plasma conditions of relevance for acceleration in flares, the fact that the reconnection configuration we studied naturally results in energetic particle jets may be of importance in other astrophysical contexts.

Subject headings: acceleration of particles — Sun: flares

1. INTRODUCTION

Magnetic reconnection has been put forward as an efficient mechanism for particle acceleration in a variety of astrophysical contexts, including solar flares, the Earth's magnetotail, active galactic nuclei (Birk et al. 2001), and pulsars (de Gouveia Dal Pino & Lazarian 2000). Understanding the origin of high-energy ions and electrons observed in flares is a major unsolved problem in solar physics (Miller et al. 1997); since the primary energy release in flares is almost certainly due to magnetic reconnection, this is a strong candidate as a mechanism for particle acceleration.

The test particle approach is widely used to investigate particle acceleration due to reconnection. It is based on calculating the trajectories of noninteracting particles in prescribed fields representative of magnetic reconnection scenarios. The majority of test particle studies of acceleration during reconnection have been carried out within a two-dimensional framework, in which uniformity of all physical parameters along one spatial direction is assumed. A large body of work exists on modeling acceleration during reconnection in two dimensions, for typical flare conditions (e.g., Browning & Vekstein 2001, Hamilton et al. 2003, and references therein). Solar jets observed in X-rays (e.g., Alexander & Fletcher 1999 and references therein) have also been ascribed to magnetic reconnection and have been modeled using two-dimensional MHD codes (Yokoyama & Shibata 1995).

In recent years, much effort has been devoted to extending the theory of magnetic reconnection to three-dimensional regimes. The simplest three-dimensional reconnection configuration is at a magnetic null. The structure of the plasma flow and fields in the vicinity of a three-dimensional magnetic null have been investigated, and two types of reconnection have been shown to occur: *spine* and *fan* reconnection (Lau & Finn 1990; Priest & Titov 1996). Three-dimensional magnetic null points are observed in the solar corona, for example, during flares (Aulanier et al. 2000; Fletcher et al. 2001) and should arise naturally due to the complex nature of the photospheric flux sources of coronal magnetic fields.

This Letter is concerned with analysis of acceleration of particles at a three-dimensional null point in the spine reconnection regime, by means of numerical integration of the trajectories of a population of test particles. We consider the reconnection configuration derived by Priest & Titov (1996), describing the electric and magnetic fields in the ideal region where resistive effects can be neglected. The trajectories of a single particle in this configuration were discussed by Dalla & Browning (2005). In the present Letter, we derive distributions of final positions of accelerated particles as well as the time evolution of their energy spectra.

While a more detailed description of the resistive region will be the subject of future work, for plasmas of large magnetic Reynolds number, as is the case, for example, in the solar corona, the volume of this region for spine reconnection is much smaller than the total volume considered in the simulation, so that from the point of view of a distribution of particles, the fraction of particles entering the resistive region will be small. As our results show, our simple model is sufficient to capture what appears to be a natural property of the configuration, namely, the fact that the escaping particles are collimated into two symmetric jets along the spine.

2. TRAJECTORIES OF A POPULATION OF PARTICLES

We obtain particle trajectories by numerically solving the relativistic equations of motion of a particle in given steady state magnetic and electric fields $\boldsymbol{B}$ and $\boldsymbol{E}$. Our code calculates full particle orbits, that is, no gyroaveraging is involved. The magnetic configuration is that of a potential three-dimensional null (Lau & Finn 1990), given in cylindrical coordinates (R, ϕ, z) by

$$\boldsymbol{B} = B_0 \frac{R}{L} \boldsymbol{e}_R - 2B_0 \frac{z}{L} \boldsymbol{e}_z, \tag{1}$$

where L is the size of the reconnection region, B_0 is the magnitude of $\boldsymbol{B}$ at $R = L$ and $z = 0$, and $\boldsymbol{e}_R$ and $\boldsymbol{e}_z$ indicate unit vectors in cylindrical coordinates. Figure 1*a* shows a plot of the magnetic field lines given by equation (1), having cylindrical symmetry about the z-axis, called the spine (Priest & Titov 1996). In the Cartesian x-y plane, the field lines are straight lines through the null describing a fan; hence, it is called the fan plane. By imposing continuous flows of plasma over a cylindrical boundary enclosing the null, and solving the steady state ideal MHD equations, Priest & Titov (1996) found analytical expressions for the flow velocity and electric field associated with reconnection. Two possible regimes were identified: spine and fan reconnection. In spine reconnection, the

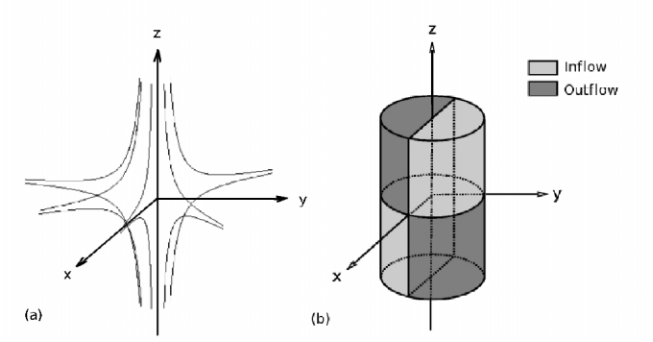

FIG. 1.—(*a*) Magnetic field lines for the potential three-dimensional magnetic null configuration. (*b*) Diagram of the inflow and outflow regions.

direction of plasma flow is within planes through the spine, and the electric field takes the form

$$\boldsymbol{E} = E_0 L \frac{\sin\phi}{R}\boldsymbol{e}_\phi, \tag{2}$$

where ϕ is the azimuthal cylindrical coordinate, also referred to in the following as longitude; E_0 is the electric field magnitude at $R = L$ and $\phi = 90°$ (value of ϕ for which the electric field is maximum). The inflow and outflow regions for the spine reconnection configuration are shown in Figure 1*b*.

Initial analysis of the trajectory of a single particle in the fields given by equations (1) and (2) showed that efficient particle acceleration can take place and that the energy gain is strongly dependent on the initial position and velocity of the particle (Dalla & Browning 2005).

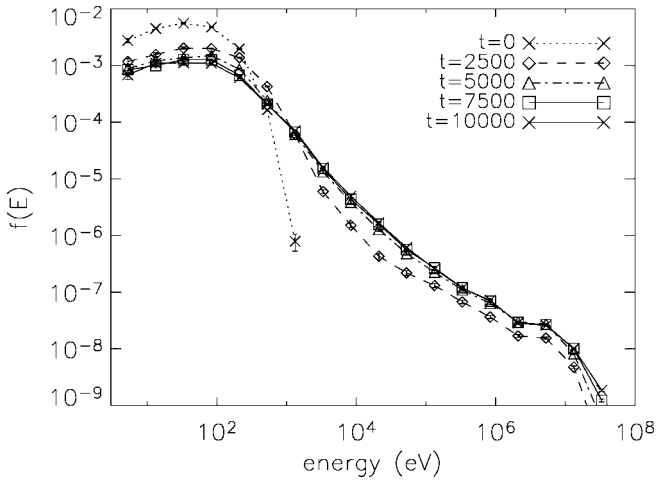

FIG. 2.—Time evolution of the energy spectrum.

Here we inject a population of particles on a spherical boundary at a distance $r = 1$ from the null point (in our code, distances are normalized by the characteristic length L, the magnetic field by B_0, and times by the nonrelativistic gyroperiod associated with a magnetic field of magnitude B_0: $T = 2\pi m_0 c/|q|B_0$, where c is the speed of light, and m_0 and q are the particle's rest mass and charge). Particles are randomly distributed on the $r = 1$ sphere at the initial time $t = 0$, and their trajectory integrated

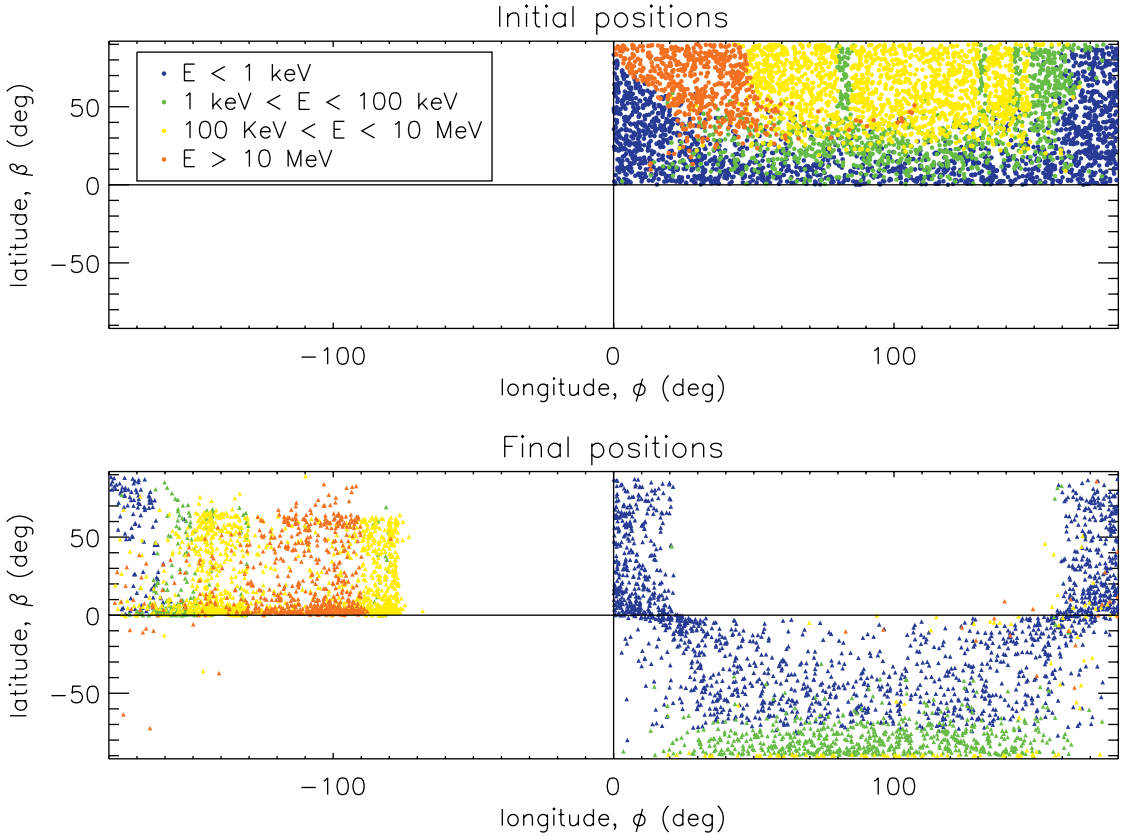

FIG. 3.—Initial and final positions of particles, plotted for particles with positive initial values of ϕ and color coded according to the final energy reached by each particle.

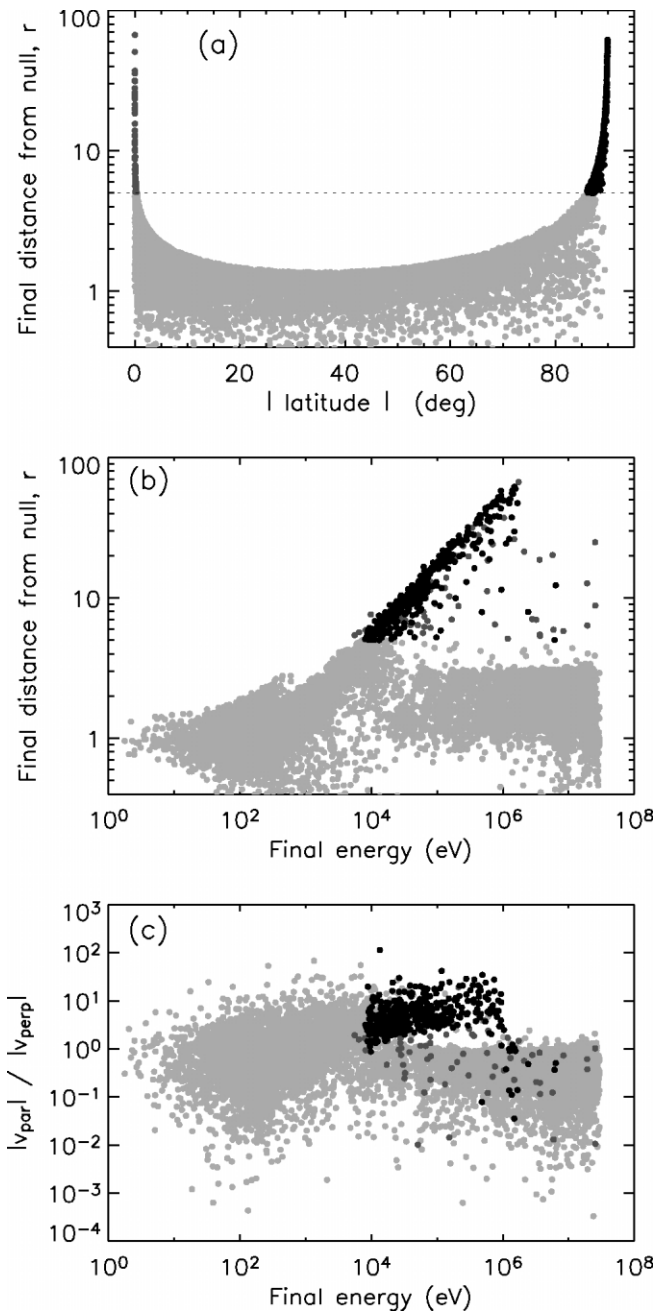

FIG. 4.—(*a*) Distance from the null vs. absolute value of latitude at the final time. (*b*) Distance from the null vs. particle energy. (*c*) Ratio of the magnitude of the component of velocity parallel to the magnetic field to perpendicular component, vs. particle energy. Black points indicate particles with $r > 5$ and large $|\beta|$, dark gray points those with $r < 5$ and small $|\beta|$, and light gray points all the other particles.

only if their initial position is in an inflow region, i.e., in one of the light gray regions in Figure 1*b*. The initial velocity components of each particle are also randomly generated according to a Maxwellian distribution.

We inject 10,000 protons into the configuration, with an initial Maxwellian temperature $T = 86$ eV ($=10^6$ K). The results presented here do not change significantly when the number of particles injected is halved. We use $B_0 = 100$ G, $E_0 = 1.5$ kV m^{-1}, and scale length $L = 10$ km, representative of the solar corona. As pointed out by Fletcher et al. (2001), the size of the reconnection region is much smaller than the overall solar flare volume; hence, we choose a value of L much smaller than the size of flare regions, allowing reasonable integration times.

The trajectory of each of the particles in our population is integrated up to a final time $t_{\rm final} = 10{,}000$. This corresponds to 64 ms, for the parameters used in the calculation. Figure 2 shows the evolution of the energy distribution of the particles, from the initial Maxwellian with $T = 86$ eV to a distribution with an effective temperature of 94 keV. The time required for a quasi–steady state to be reached is around a few thousand gyroperiods. The high-energy part of the spectrum is well fitted by a power law $f(E) \propto E^{-\gamma}$ with spectral index $\gamma = 0.92$. The bump that is observed at high energies is the result of a fraction of the particles being able to reach the region close to the spine where acceleration is most efficient. Our analysis of single particle trajectories showed that this feature is associated with the existence of an optimal injection angle (see Fig. 4 of Dalla & Browning 2005), for which the highest energies are reached.

Figure 3 shows the angular location of the particles in our population at the initial time (*top plot*) and the final time (*bottom plot*). Each location is identified by its latitude β, i.e., the elevation angle from the *x*-*y* plane, and longitude ϕ. Inflow regions are the top right and bottom left quadrants in the ϕ, β representation (see Fig. 1*b*). In Figure 3, we only show the initial and final positions of particles starting in the top right inflow region. Particles (not shown) starting in the bottom left quadrant have distributions of initial and final positions symmetric with respect to those shown in Figure 3, apart from statistical fluctuations. While the distance from the null at the initial time is the same for all particles ($r = 1$), at the final time this distance varies within our population, as is discussed in § 3. Each point of Figure 3 is color coded according to the final particle energy. This allows us to identify which initial locations in the inflow region will result in low/mid/high/very high final energy. It also allows identification of preferred exit locations for the various energy ranges. Particles represented by blue dots are not strongly accelerated: at the final time, either they are in the bottom right outflow region or they are still in the inflow region, since they were injected in locations near $\phi = 0°$ and $\phi = 180°$, where the inflow speed is small. Particles color coded in green, yellow, and red are accelerated, and their final position is in one of the outflow regions. For a fixed plane of injection ϕ, the optimal injection angle ($\beta = 35°$) found for single particle trajectories (Dalla & Browning 2005) can be seen. At a fixed latitude, the final energy was shown to increase as the plane of injection ϕ decreases from 180° to 0°; this is also clear from Figure 3, except that the low-energy (*blue*) particles near $\phi = 0°$ have not been accelerated within the simulation time.

3. TRAPPED AND ESCAPING POPULATIONS

Figure 3 only gives information on the angular location of the final position of the particles. Another very important parameter to be taken into consideration is the spherical distance r at the final time.

Figure 4*a* shows a plot of the distance of particles from the null versus magnitude of the latitude β at the final time of integration. One can observe that particles with large values of r are located either at very high $|\beta|$ (near the spine) or at very low $|\beta|$ (near the fan plane). In all panels of Figure 4, we color coded these particles into two groups: the black points are those with $r > 5$ and large $|\beta|$ and the dark gray ones those

with $r > 5$ and small $|\beta|$. The first group consists of 392 particles (4% of the total particle number), and the second one of 69 particles (0.7% of the total number). The former group of escaping energetic particles correspond to green and yellow points in the bottom right quadrant of the final positions panel in Figure 3 (and their counterpart, not shown in Figure 3, in the opposite outflow quadrant). The latter low $|\beta|$ group are represented by yellow and red points in the top left outflow quadrant of Figure 3.

Figure 4*b* shows the final distance from the null versus final particle energy: the majority of particles with large values of r have energies in the range 10 keV–1 MeV. Particles accelerated to the highest energies (>1 MeV) tend to remain within $r \approx 3$. Figure 4*c* shows the ratio of the magnitudes of the particles' velocity components parallel and perpendicular to the magnetic field direction, versus the final energy. The majority of black particles also tend to have $|v_{\rm par}| > |v_{\rm perp}|$.

Combining all the information in the panels of Figure 4, we identify the presence of two energetic particle populations: a trapped population and an escaping one. The trapped particles remain within a sphere of radius $r \approx 3$ from the null and are characterized by the largest energies and a small ratio of $|v_{\rm par}|/|v_{\rm perp}|$. Analysis of individual trajectories shows that they display a mirroring motion associated with conservation of the magnetic moment. Locating the dark gray particles in Figure 4*c*, we can see that a significant fraction of particles in this group are trapped. The escaping population are found at large distances from the null at the final time and have a large ratio of $|v_{\rm par}|/|v_{\rm perp}|$. They tend to be black points in Figure 4; hence, they are mainly escaping at high $|\beta|$.

We conclude that the majority of the accelerated particles that escape from the configuration are propagating at large positive and large negative values of the latitude, in two energetic particle jets along the spine.

4. DISCUSSION

Our analysis of test particle acceleration during spine reconnection at a three-dimensional magnetic null shows for the first time that this configuration produces two symmetric jets of energetic particles escaping along the spine. For the parameters we used, the jets are highly collimated at latitudes above 80°. We also showed that a population of trapped particles is produced. The average energy of the escaping population is lower than that of the trapped one. The spectrum produced can be approximated by a power law of spectral index 0.92. The maximum proton energies obtained in our simulation (~10 MeV) and acceleration timescale of ~60 ms are broadly consistent with solar flare observations (Miller et al. 1997).

The Priest & Titov (1996) treatment fails to describe the high-current cylindrical region near the spine where resistive and other nonideal effects need to be taken into account. For plasmas in the solar corona, the size of this region is small due to the very large values of the magnetic Reynolds number. Hence, the electric field of equation (2) is an approximation that describes accurately the trajectories of a majority of particles, except those that enter the resistive region. It should be pointed out that the use of more accurate fields derived from resistive equations would probably modify the characteristics of the trapped population. It would not, however, change our conclusions as far as the escaping population is concerned, since the majority of the jet particles remain at significant distances from the spine, and their characteristics are properly described by the model fields used in our simulation. As a further test of this, we ran our model with a modified electric field as described in § 9 of Dalla & Browning (2005), where the electric field is constant inside a cylindrical region of radius $L_{\rm spine}$ around the spine. We found that values of $L_{\rm spine} = 0.001$ and 0.01 (normalized to the size of the region L) did not modify the properties of the escaping jets.

It is interesting to discuss how the characteristics of the jets along the spine change when the magnitude of the magnetic field B_0 is varied, keeping all other parameters constant. If we double the magnetic field, the efficiency of acceleration decreases significantly, as a result of the average electric drift speed $v_E = cE_0/B_0$ decreasing. Some acceleration is observed in the energy range 1 keV–1 MeV; however, no jets are produced.

Halving the value of B_0 results in very efficient acceleration, over shorter timescales than those seen in Figure 2 and producing a similar spectral index. The jets produced are less collimated than those of Figure 4 and contain a larger fraction of the particles. Increasing/decreasing the electric field has the inverse effect, because of the scaling with the drift speed.

It is useful to place our results within the context of observational evidence for three-dimensional null points during solar flares. Figure 9 of Aulanier et al. (2000) shows the magnetic field lines obtained from potential extrapolation of photospheric magnetic fields, where the spine line of the three-dimensional null connects down to lower regions in the corona. The jets of energetic particles generated by spine reconnection in such a configuration would be responsible for so-called footpoint emission, after traveling along the spine down to regions of denser plasma. It seems possible that the trapped population may be responsible for the so-called looptop flare emission. Both observational papers that report detection of a three-dimensional magnetic null configuration in association with flares describe the observed active region as characterized by a concentration of field of one polarity surrounded by the field of the opposite polarity (δ-spot; Aulanier et al. 2000; Fletcher et al. 2001).

In addition to the magnetic configuration that we considered, a variety of nonaxisymmetric three-dimensional nulls exist (Parnell et al. 1996), for which acceleration due to reconnection needs to be investigated. It seems likely, however, that the spine will provide a natural escape for accelerated particles in these configurations too. We cannot say at this stage whether jets of energetic particles would be produced by the other possible reconnection regime at a three-dimensional null point, fan reconnection, but this will be the subject of future investigation.

REFERENCES

Alexander, D., & Fletcher, L. 1999, Sol. Phys., 190, 167
Aulanier, G., DeLuca, E. E., Antiochos, S. K., McMullen, R. A., & Golub, L. 2000, ApJ, 540, 1126
Birk, G. T., Crusius-Wätzel, A. R., & Lesch, H. 2001, ApJ, 559, 96
Browning, P. K., & Vekstein, G. E. 2001, J. Geophys. Res., 106, 18677
Dalla, S., & Browning, P. K. 2005, A&A, 436, 1103
de Gouveia Dal Pino, E. M., & Lazarian, A. 2000, ApJ, 536, L31
Fletcher, L., Metcalf, T. R., Alexander, D., Brown, D. S., & Ryder, L. A. 2001, ApJ, 554, 451
Hamilton, B., McClements, K. G., Fletcher, L., & Thyagaraja, A. 2003, Sol. Phys., 214, 339
Lau, Y.-T., & Finn, J. M. 1990, ApJ, 350, 672
Miller, J. A., et al. 1997, J. Geophys. Res., 102, 14631
Parnell, C. E., Smith, J. M., Neukirch, T., & Priest, E. R. 1996, Phys. Plasmas, 3, 759
Priest, E. R., & Titov, V. S. 1996, Philos. Trans. R. Soc. London A, 354, 2951
Yokoyama, T., & Shibata, K. 1995, Nature, 375, 42